IAHR AIRH

Journal of Hydraulic Research Vol. 43, No. 1 (2005), pp. 56–70

The dynamic effect of pipe-wall viscoelasticity in hydraulic transients. Part II— model development, calibration and verification

L'effet dynamique de la viscoélasticité de la conduite en régimes transitoires hydrauliques. Partie II—développement, calibrage and vérification du modèle mathématique

DÍDIA COVAS, *Civil Engineering Department, Instituto Superior Técnico, Av. Rovisco Pais, 1049-001 Lisbon, Portugal. E-mail: didia.covas@civil.ist.utl.pt (author for correspondence)*

IVAN STOIANOV, *Civil and Environmental Engineering Department, Imperial College of Science, Technology and Medicine, Imperial College Road, SW7 2BU, London, UK. E-mail: ivan.stoianov@ic.ac.uk*

JOÃO F. MANO, *Polymer Engineering Department, Minho University, Azurém Campus, 4800-058 Guimarães, Portugal. E-mail: jmano@dep.uminho.pt*

HELENA RAMOS, *Civil Engineering Department, Instituto Superior Técnico, Av. Rovisco Pais, 1049-001 Lisbon, Portugal. E-mail: helena.ramos@civil.ist.utl.pt*

NIGEL GRAHAM, *Civil and Environmental Engineering Department, Imperial College of Science, Technology and Medicine, Imperial College Road, SW7 2BU, London, UK. E-mail: n.graham@ic.ac.uk*

CEDO MAKSIMOVIC *Civil and Environmental Engineering Department, Imperial College of Science, Technology and Medicine, Imperial College Road, SW7 2BU, London, UK. E-mail: c.maksimovic@ic.ac.uk*

ABSTRACT
A state-of-the-art mathematical model has been developed to calculate hydraulic transients in pressurized polyethylene (PE) pipe systems. This hydraulic transient solver (HTS) incorporates additional terms to take into account unsteady friction and pipe-wall viscoelasticity. Numerical results obtained were compared with the classic waterhammer solution and with experimental data collected from a PE pipe-rig at Imperial College (London, UK). Unlike the classical model, the developed HTS is capable of accurately predicting transient pressure fluctuations in PE pipes, as well as circumferential strains in the pipe-wall. The major challenge was the distinction between frictional and mechanical dynamic effects. First, the HTS was calibrated and tested considering these two effects separately: if only unsteady friction was considered, a major disagreement between collected data and numerical results was observed; when only the viscoelastic effect was considered, despite the good agreement between data and numerical results, the calibrated creep function depended on the initial flow rate. In a second stage, the combination of these dynamic effects was analysed: creep was calibrated for laminar flow and used to test the solver for turbulent conditions, and a good agreement was observed. Finally, the HTS was tested using creep measured in a mechanical test, neglecting unsteady friction, and a good agreement was obtained.

RÉSUMÉ
Un nouveau modèle mathématique a été développé pour calculer les régimes transitoires hydrauliques des systèmes de conduites pressurisées en polyéthylène (PE). Ce modèle hydraulique (nommé HTS) intègre des termes additionnels pour simuler la friction pendant le régime transitoire et l'effet de la viscoélasticité de la conduite. Les résultats numériques obtenus ont été comparés avec la solution classique du coup de bélier et avec les résultats expérimentaux collectés à partir d'un système de conduites simples en PE construit au Imperial College (Londres, Royaume Unit). Contrairement au modèle classique, le modèle HTS est capable de prédire rigoureusement les fluctuations transitoires de pression dans la conduite de PE ainsi que l'extension de la circonférence des parois de la conduite. Le grand challenge de ce travaille est la distinction entre l'effet dynamique de la friction transitoire et l'effet mécanique de la déformation retardée de la conduite. Dans un premier temps, le modèle HTS a été calibré et testé en considérant les deux effets séparément. Lorsque la friction en régime transitoire est considérée seule, de grandes différences entre les résultats expérimentaux et numériques sont observées. Si l'effet viscoélastique de la conduite est considéré seul, même avec une bonne corrélation entre les résultats expérimentaux et numériques, les fonctions des fluage calibrées varient avec le flux initial. Dans un deuxième temps, la combinaison de ces deux effets a été analysée et une bonne correspondance entre les résultats expérimentaux et numériques a été observée. Enfin, le modèle HTS a été vérifié avec succès en utilisant la fonction de fluage mesurée lors d'un test mécanique négligeant la friction en régime transitoire.

Keywords: Hydraulic transients, transient solver, polyethylene, viscoelasticity, unsteady friction.

Revision revised December 4, 2003 / Open for discussion until August 31, 2005.

1 Introduction

Hydraulic transient analysis is important in the design of water pipeline systems for selection of pipe materials and pressure classes, and for specification of surge protection devices. Classic waterhammer theory based on the assumptions of linear elastic behaviour of pipe walls and quasi-steady-state friction losses is typically used to predict the maximum and minimum pressure surges in the fluid systems (Chaudhry, 1987; Almeida and Koelle, 1992; Wylie and Streeter, 1993). This approach is relatively accurate to describe hydraulic transients in metal or concrete pipes; however, it is considerably imprecise for plastic pipes (e.g. polyethylene), particularly in surges generated by rapid changes in flow conditions. Plastic pipes, such as polyethylene (PE) and polyvinyl chloride (PVC), have been increasingly used in water supply systems due to their high resistant properties (mechanical, chemical, temperature and abrasion) and cost-effective price. Polymers, in general, exhibit a viscoelastic mechanical behaviour (Ferry, 1970; Aklonis *et al.*, 1972; Riande *et al.*, 2000) that influences the pressure response of the pipe system during transient events. This behaviour is not usually properly accounted for in systems design, as transient events are evaluated either by rules of thumb or by classical transient simulators. The assumptions associated with these formulations are unrealistic in plastic pipe systems, particularly for fast transient events.

In this context, a novel Hydraulic Transient Simulator (HTS), which incorporates additional terms to take into account unsteady friction and two types of mechanical behaviours of the pipe-wall (linear-elastic or linear-viscoelastic), has been developed. This HTS was calibrated and tested using transient pressure and circumferential strain data. These data were collected from a single high-density PE pipe-rig at Imperial College as described in the companion paper (Covas *et al.*, 2004). In an attempt to distinguish unsteady friction from the effect of pipe-wall viscoelasticity, four different approaches were used to test the developed HTS. First, the HTS was tested considering only unsteady friction effects. Second, creep function was calibrated neglecting unsteady friction. Third, the transient solver was calibrated for laminar flow considering Trikha's (1975) unsteady friction formulation and the calibrated solver was tested for turbulent conditions. Finally, the HTS was tested neglecting unsteady friction and using the creep-function determined experimentally in an independent mechanical test in the companion paper (Covas *et al.*, 2004). Conclusions are drawn concerning the importance of the incorporation of this mechanical behaviour in a hydraulic transient model in plastic pipes.

2 Background review

2.1 Unsteady friction

Unsteady-friction losses have been widely studied for the last 50 years. These losses are particularly evident in linear elastic materials, like concrete, metal and asbestos cement during fast transient events or high-oscillating frequencies. Whilst unsteady friction can be reasonably well described for laminar flow (Zielke, 1968; Trikha, 1975), no universally accepted formula has been developed yet for turbulent conditions. Several formulations for unsteady friction calculation have been presented, in the literature, assuming that these losses depend on: (i) instantaneous mean velocity (Hino *et al.*, 1976, 1977); (ii) instantaneous acceleration (Daily *et al.*, 1956; Carstens and Roller, 1959; Safwat and Polder, 1973; Shuy, 1996); (iii) weights of past time local accelerations (Zielke, 1968; Trikha, 1975; Suzuki *et al.*, 1991; Vardy, 1992; Vardy *et al.*, 1993; Vardy and Brown, 1995, 1996); (iv) local and convective acceleration (Brunone *et al.*, 1991, 1995; Vitkovsky *et al.*, 2000; Bergant *et al.*, 2001); and (v) velocity profiles (Bratland, 1986; Vardy and Hwang, 1991; Eichinger and Lein, 1992; Silva-Araya and Chaudhry, 1997; Pezzinga, 1999, 2000).

The numerical results obtained by these formulations were, in most cases, compared with data collected in metal or concrete pipes, typically with a linear-elastic mechanical behaviour. Transient data collected by Holmboe and Rouleau (1967) in a steel pipe and in a copper pipe embedded in concrete were used as benchmark tests over many years. More recently, Brunone *et al*. (1999, 2000) carried out experimental tests in a 350-m PE pipe-rig and attributed the observed pressure wave dampening to unsteady friction losses. These authors attempted to describe the observed pressure dampening by using an extremely high decay coefficient used in Brunone's unsteady friction formula (Brunone *et al.*, 1995). The obtained numerical results presented large discrepancies with experimental data both in terms the general shape of the pressure signal and of the amplitude and phase of the pressure wave. It is believed that the reason for these results was that these authors neglected the dynamic effect of pipe-wall viscoelasticity.

2.2 Pipe-wall viscoelasticity

Although the viscoelastic behaviour of polymers is well known, this behaviour tends to be forgotten in hydraulic transient analysis in plastic pipes. The viscoelastic behaviour is characterized by an instantaneous elastic strain followed by a gradual retarded strain for an applied load. This retarded behaviour of pipe-wall causes a significant attenuation of the transient pressure oscillation and increases the dispersion of the pressure wave. Two different approaches have been proposed to describe this behaviour in hydraulic transient solvers: a frequency-dependent wave speed and an additional viscoelastic term added to the mass balance fluid equation.

The concept behind the frequency-dependent wave speed is that the viscoelastic behaviour of the pipe-wall is time (or frequency) dependent, and, in the frequency domain, it can be reasonably well described in terms of the angular frequency ($\omega = 2\pi/t$). Consequently, the modulus of elasticity E_0 of the pipe material used in the wave speed calculation is replaced by the inverse of the creep function, J (Covas *et al.*, 2004) (the creep-function is equal to the inverse modulus of elasticity, $J_0 = 1/E_0$ in time-independent phenomena). Meißner and Franke (1977) investigated the damping of steady-oscillatory flows in PVC and steel pipes. The viscoelastic attenuation of

the pressure surges was much higher than the friction damping (although they did not account for unsteady skin friction). These authors derived the wave speed and the damping factor formulae for an oscillating pressure in a thin-walled viscoelastic pipe. Rieutford (1982) analysed laminar transient flow in viscoelastic pipes and proposed a "one Kelvin–Voigt element" model to describe the creep-function and to include in the wave speed formula. Franke and Seyder (1983) incorporated Meißner and Franke's wave speed formulas in unsteady fluid equations, and solved these by the Impedance Method, for steady-oscillatory flows, and by the Impulse Response Method, for non-periodic flows. Suo and Wylie (1990a) modelled pipe-wall viscoelasticity in both oscillatory and non-periodic flows. Suo and Wylie (1990b) analysed frequency-dependent wave speed in a rock-bored tunnel due to the dynamic effect of the surrounding rock mass.

The use of the additional viscoelastic term is related to the rheology of the viscoelastic materials in which there is an instantaneous-elastic response (accounted for in the elastic wave speed) and a retarded-viscoelastic response. This retarded behaviour is described by an additional time-dependent term that is incorporated into the mass-balance equation. This formulation has been proposed by Rieutford and Blanchard (1979) and Gally *et al.* (1979). Rieutford and Blanchard (1979) described this model in viscoelastic pipes and theoretically analysed the effect of the relaxation times of a "three Kelvin–Voigt element" model. Gally *et al.* (1979) experimentally determined the creep-function by dynamic tests and verified the model with pressure and circumferential-strain data collected in a single PE pipeline. A slight disagreement in the strain data and numerical results was observed. Ghilardi and Paoletti (1986) showed that the viscoelastic dampening could be usefully used to reduce pressure surges. Rachid and Stuchenbruck (1990) modelled viscoelastic pipe behaviour coupled and uncoupled with fluid–structure interaction. Rachid *et al.* (1992) implemented several types of non-elastic rheological behaviour. Pezzinga (2002) analysed the effect of an additional PE pipe downstream of a pump to reduce induced pressure surges.

3 Model development

3.1 Linear-elastic model

The theoretical fundamentals of transient analysis are common to pressurized and open-channel unsteady-state flows. The flow movement, when temperature changes are negligible, is described by the mass-balance and the momentum-conservation principles. The continuity and momentum equations that describe one-dimensional transient flow in pressurised conduits are a set of two differential equations (Chaudhry, 1987; Almeida and Koelle, 1992; Wylie and Streeter, 1993):

$$\frac{\mathrm{d}H}{\mathrm{d}t} + \frac{a_0^2}{gS}\frac{\partial Q}{\partial x} = 0 \tag{1}$$

$$\frac{\partial H}{\partial x} + \frac{1}{gS}\frac{\mathrm{d}Q}{\mathrm{d}t} + h_\mathrm{f} = 0 \tag{2}$$

where Q is the flow rate, H the piezometric head, a_0 the elastic wave speed, g the gravity due to acceleration, S the pipe cross-sectional area, x the coordinate along the pipeline axis, t the time, h_f the head loss per unit length. Several simplifying assumptions are considered in the derivation of these equations (Almeida and Koelle, 1992), and the most important are the following: (i) pseudo-uniform velocity profile (consequently, friction losses are described by steady-state formulae and coriolis and momentum coefficients are constant); (ii) the rheological behaviour of the pipe material is linear-elastic; (iii) the fluid is one-phase, homogenous and compressible; and (iv) the pipe is uniform and completely constrained from any axial or lateral movement.

In order to take into account unsteady friction losses and fluid inertial effects, corresponding to the non-verification of assumption (i), the head loss per unit length h_f is decomposed into two terms, a steady-state component h_fs, and an unsteady-state component, h_fu:

$$h_\mathrm{f} = h_\mathrm{fs} + h_\mathrm{fu} \tag{3}$$

The steady-state component h_fs is calculated for turbulent and laminar flow, respectively, by:

$$h_\mathrm{fs} = \frac{f_\mathrm{s}}{2gD}\frac{Q|Q|^{n-1}}{S^n} \quad \text{and} \quad h_\mathrm{fs} = \frac{32\nu'}{gD^2}\frac{Q}{S} \tag{4}$$

where f_s is the Darcy–Weisbach friction factor, D the pipe inner diameter, n the exponent of flow in the friction loss equation and ν' the kinematic fluid viscosity.

The unsteady component h_fu is usually neglected in the classic waterhammer analysis. Whilst this assumption is reasonably accurate for slow transients and low pulsating frequencies, rapid transient events and high pulsating frequencies require a more accurate representation of unsteady skin friction. Several unsteady friction formulations were implemented in the developed HTS: Trikha's (1975), Vardy *et al.*'s (1993) and Brunone *et al.*'s (1995).

Trikha's (1975) formula is a simplification of Zielke's (1968) and is quite accurate for laminar flows (Fig. 1a):

$$h_\mathrm{fu} \approx \frac{16\nu}{gD^2}[Y_1 + Y_2 + Y_3] \quad \text{with}$$

$$Y_i(t) = Y_i(t-\Delta t)\mathrm{e}^{-n_i(4\nu/D^2)\Delta t} + m_i[V(t) - V(t-\Delta t)] \tag{5a}$$

Parameters n_i and m_i are null for steady state, and $m_1 = 40$, $n_1 = -8000$, $m_2 = 8.1$, $n_2 = -200$, $m_3 = 1$ and $n_3 = -26.4$, during the transient event.

Vardy *et al.*'s (1993) formula has a similar form as Trikha's, though with only two terms Y_i and it was developed for smooth-wall turbulent flows:

$$h_\mathrm{fu} \approx \frac{16\nu}{gD^2}[Y_1 + Y_2] \quad \text{with}$$

$$Y_i(t) = Y_i(t-\Delta t)\mathrm{e}^{-B_i(4\nu/D^2)\Delta t} + A_i[V(t) - V(t-\Delta t)] \tag{5b}$$

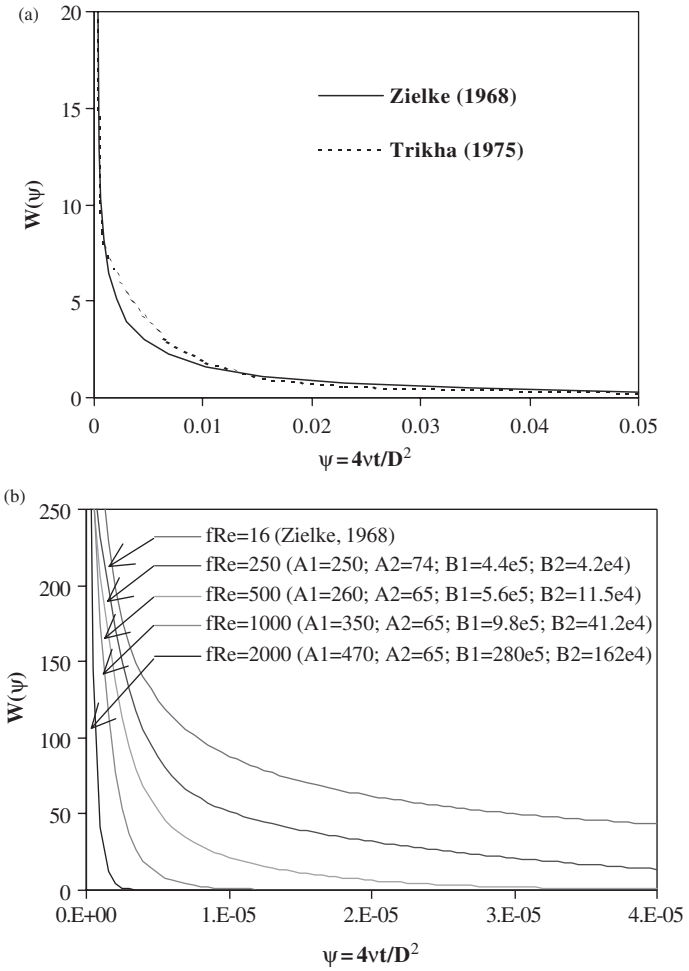

Figure 1 (a) Comparison between Zielke's and Trikha's weighting functions for laminar flows. (b) Family of weighting functions for smooth wall flows with low *Re* (Vardy *et al.*, 1993).

Parameters A_i and B_i depend on the product of friction and Reynolds number ($f \times Re$) and the respective weighting functions are presented in Fig. 1b. Zielke's (1968) exact formulation for laminar flows is an upper bound of these weighting functions developed for smooth-wall turbulent flows. The values of $f \times Re$ of transient tests carried out in this work are within the range of suggested values by the authors, i.e. $f \times Re \leq 2000$ (Fig. 1b):

Brunone *et al.*'s (1995) formula, with Vitkovsky *et al.*'s improvement (Vitkovsky *et al.*, 2000), provides better results for turbulent flows:

$$h_{\mathrm{fu}} = \frac{k'}{gS}\left(\frac{\partial Q}{\partial t} + a_0 SGN(Q)\left|\frac{\partial Q}{\partial x}\right|\right) \tag{6}$$

where k' is Brunone's decay coefficient and *SGN* the operator for the sign of the average velocity. This formula relies on the calibration of the decay coefficient based on collected transient data.

The elastic wave speed, a_0, is a parameter that depends on the fluid compressibility, and on the physical properties and external constraints of the conduit. Assuming a linear-elastic behaviour of the pipe-wall (described by Hooke's law), wave speed can be estimated by (Chaudhry, 1987):

$$a_0 = \sqrt{\frac{K/\rho}{1 + (\alpha D/e)(K/E_0)}} \tag{7}$$

where E_0 is Young's modulus of elasticity of the pipe, K the bulk modulus of elasticity of the fluid, ρ the fluid density, e the pipe-wall thickness and α the dimensionless parameter that depends on the cross-section dimensions and on pipe axial constraints (Chaudhry, 1987; Wylie and Streeter, 1993). The calculation of parameter α is presented in the companion paper for a thick-walled pipe.

3.2 Linear-viscoelastic model

Polyethylene pipes have a different rheological behaviour in comparison to metal and concrete pipes. When subjected to a certain instantaneous stress σ_0, polymers do not respond according to Hooke's law: plastics have an immediate-elastic response and a retarded-viscous response. In this way, strain can be decomposed into an instantaneous-elastic strain, ε_{e}, and a retarded strain, ε_{r} (Fig. 2a):

$$\varepsilon(t) = \varepsilon_{\mathrm{e}} + \varepsilon_{\mathrm{r}}(t) \tag{8a}$$

According to "Boltzmann superposition principle", for small strains, a combination of stresses that act independently in a system result in strains that can be added linearly. This is presented in Fig. 2(b) for the particular case of two stresses. Thus, the total strain generated by a continuous application a stress $\sigma(t)$ is (Aklonis *et al.*, 1972):

$$\varepsilon(t) = J_0\sigma(t) + \int_0^t \sigma(t - t')\frac{\partial J(t')}{\partial t'}\mathrm{d}t' \tag{8b}$$

in which J_0 is the instantaneous creep-compliance and $J(t')$ the creep function at t' time. For linear-elastic materials, creep-compliance J_0 is equal to the inverse modulus of elasticity, $J_0 = 1/E_0$.

Assuming that the pipe material is (i) homogeneous and isotropic, (ii) it has linear viscoelastic behaviour for small strains,

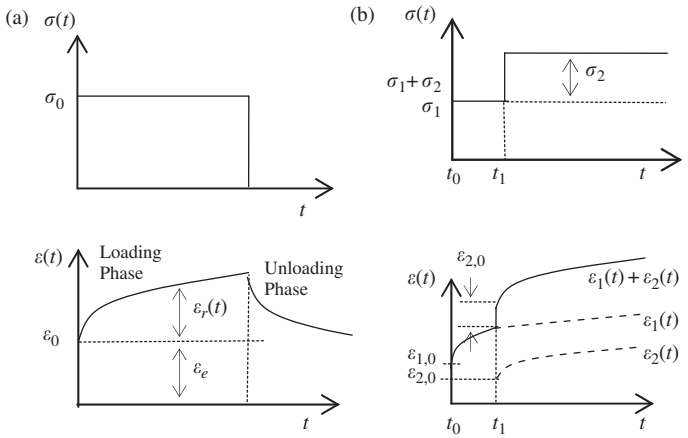

Figure 2 (a) Stress and strain for an instantaneous constant load. (b) Boltzmann superposition principle for two stresses applied sequentially.

(iii) Poisson's ratio ν is constant so that the mechanical behaviour is only dependent on a creep-function, and (iv) circumferential-stress σ is given by $\sigma = \alpha \Delta p D/2e$, the total circumferential strain, $\varepsilon = (D - D_0)/D_0$, is described by:

$$\varepsilon(t) = \frac{\alpha_0 D_0}{2e_0}[p(t) - p_0]J_0 + \int_0^t \frac{\alpha(t-t')D(t-t')}{2e(t-t')}[p(t-t') - p_0]\frac{\partial J(t')}{\partial t'}\mathrm{d}t' \tag{9}$$

where $p(t)$ is the pressure at time t, p_0 the initial pressure, J_0 the instantaneous creep-compliance, $J(t)$ the creep-compliance function at time t, $D(t)$ and D_0 the inner diameters at time t and $t = 0$, respectively, $e(t)$ and e_0 the wall thicknesses at time t and $t = 0$, respectively; $\alpha(t)$ and α_0 the pipe-wall constraint coefficient at time t and $t = 0$, respectively. The first term of Eq. (9) corresponds to the elastic strain ε_e and the integral part to the retarded strain ε_r. The creep-compliance function $J(t)$, which describes the viscoelastic behaviour of the pipe material, can be determined experimentally in an independent mechanical test (Covas, 2003; Covas *et al.*, 2004), or calibrated based on collected transient data. Afterwards, this function should be represented by a mathematical expression that can be implemented numerically.

In order to take into account the viscoelastic behaviour of the pipe-wall, the continuity equation (Eq. 1) has to be obtained again from the Reynolds transport theorem. Taking into account the relationship between cross-sectional area, S, and total strain, ε (i.e. $\mathrm{d}S/\mathrm{d}t = 2S\mathrm{d}\varepsilon/\mathrm{d}t$), and the two components of strain, $\varepsilon = \varepsilon_\mathrm{e} + \varepsilon_\mathrm{r}$ (ε_e is the elastic strain and ε_r the retarded strain), the continuity equation yields (Covas, 2003):

$$\frac{\mathrm{d}H}{\mathrm{d}t} + \frac{a_0^2}{gS}\frac{\partial Q}{\partial x} + \frac{2a_0^2}{g}\frac{\mathrm{d}\varepsilon_r}{\mathrm{d}t} = 0 \tag{10}$$

Whilst the third term represents the retarded effect of pipe-wall, the elastic strain is included in the piezometric head time derivative and in the elastic wave speed, a_0. The elastic wave speed is calculated by Eq. (7) considering $E_0 = 1/J_0$. Equation (10) solved with Eq. (2) and the second term of Eq. (9) describes the pressure-flow fluctuations along a pressurized pipe. For viscoelastic pipes, a new concept of wave speed, a, can be defined in terms of the creep-compliance function (Covas, 2003). This wave speed is a time-dependent parameter that decreases during the transient event, as a result of the increase of the creep-function. This justifies the pressure wave dampening and phase shift during the propagation of the transient event.

3.3 Numerical scheme for the viscoelastic model

The set of differential equations (10) and (2) is solved by the Method of Characteristics (MOC). The stability of this method requires the verification of a numerical restriction for the time and space steps, given by the Courant–Friedrich–Lewy stability condition, $\mathrm{d}x/\mathrm{d}t = V \pm a_0$, which corresponds to the propagation of flow features along curved characteristic lines. This condition allows the transformation of Eqs (9) and (2) into a set of total differential equations:

$$\frac{\mathrm{d}H}{\mathrm{d}t} \pm \frac{a_0}{gS}\frac{\mathrm{d}Q}{\mathrm{d}t} + \frac{2a_0^2}{g}\left(\frac{\partial \varepsilon_r}{\partial t}\right) \pm a_0 h_f = 0 \tag{11}$$

valid along the characteristic lines $\mathrm{d}x/\mathrm{d}t = V \pm a_0$. For the linear-elastic case, the retarded strain–time derivative is null. The numerical resolution of these complete equations (including convective terms) requires the use of a characteristic grid (Gally *et al.*, 1979), or interpolations in a rectangular double grid. Whilst the characteristic grid is difficult to compactibilize at nodes in systems with multiple pipes, the rectangular grid requires the use of interpolations that introduce artificial numerical damping in the pressure response (Wylie and Streeter, 1993).

In most engineering problems when the fluid is water, the fluid velocity is negligible compared to elastic wave speed ($V \ll a_0$). Thus, the set of Eqs (11) is further simplified by neglecting convective terms, leading to approximately straight characteristic lines $dx/dt = \pm a_0$. These simplified equations can be solved by the following numerical scheme:

$$\begin{aligned}&\big[H(x,t) - H(x \mp \Delta x, t - \Delta t)\big] \\ &\quad \pm \frac{a_0}{gS}\big[Q(x,t) - Q(x \mp \Delta x, t - \Delta t)\big] \\ &\quad + \frac{2a_0^2 \Delta t}{g}\left(\frac{\partial \varepsilon_r}{\partial t}\right) \pm a_0 \Delta t h_f = 0\end{aligned} \tag{12}$$

valid along the characteristic lines $\mathrm{d}x/\mathrm{d}t = \pm a_0$. In these equations, there are two terms that cannot be directly calculated and that require further numerical discretization: the retarded strain time-derivative and the slope of the energy line.

The time-derivative of the retarded strain is calculated by deriving the second term of Eq. (9). The creep function of the pipe-wall should be represented by a mathematical expression in order to be able to analytically calculate this derivative. The mechanical model of a generalized viscoelastic solid (Fig. 3) is typically used to describe the creep function (Aklonis *et al.*, 1972):

$$J(t) = J_0 + \sum_{k=1}^{N} J_k(1 - \mathrm{e}^{-t/\tau_k}) \tag{13}$$

where J_0 is the creep-compliance of the first spring defined by $J_0 = 1/E_0$, J_k the creep-compliance of the spring of the Kelvin–Voigt k-element defined by $J_k = 1/E_k$, E_k the modulus of elasticity of the spring of k-element, τ_k the retardation time of the dashpot of k-element, $\tau_k = \eta_k/E_k$, η_k the the viscosity of the dashpots of k-element. The parameters J_k and τ_k of the viscoelastic mechanical model are adjusted to the creep-compliance experimental data. According to this mathematical

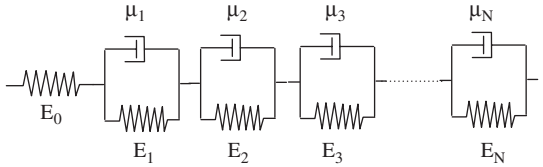

Figure 3 Generalized Kelvin–Voigt Model (viscoelastic solid).

model, the terms $\partial\varepsilon_r/\partial t$ and ε_r are calculated as the sum of these factors for each Kelvin–Voigt element k:

$$\varepsilon_{\mathrm{r}}(x,t) = \sum_{k=1,\ldots,N} \varepsilon_{\mathrm{r}k}(x,t) = \sum_{k=1,\ldots,N} \left\{ \frac{\alpha D}{2e}\gamma \int_0^t \big[H(x,t-t') - H_0(x)\big] \frac{J_k}{\tau_k} \mathrm{e}^{\frac{-t'}{\tau_k}} \mathrm{d}t' \right\} \tag{14}$$

$$\frac{\partial\varepsilon_{\mathrm{r}}(x,t)}{\partial t} = \sum_{k=1,\ldots,N} \frac{\partial\varepsilon_{\mathrm{r}k}(x,t)}{\partial t} = \sum_{k=1,\ldots,N} \left\{ \frac{\alpha D}{2e}\frac{J_k}{\tau_k}\gamma\big[H(x,t) - H_0(x)\big] - \frac{\varepsilon_{\mathrm{r}k}(x,t)}{\tau_k} \right\} \tag{15}$$

Considering the creep function defined by the generalized viscoelastic solid model (Eq. 13) and introducing the time-derivative of this function $J(t)$ in the second term of Eq. (9), it yields for each Kelvin–Voigt element k:

$$\varepsilon_{\mathrm{r}k}(x,t) = \int_0^t F(x,t-t')\frac{J_k}{\tau_k}\mathrm{e}^{-t'/\tau_k}\mathrm{d}t' \tag{16}$$

where the function $F(x,t)$ is defined by:

$$F(x,t) = \frac{\alpha D}{2e}\gamma\big[H(x,t) - H_0(x)\big] \tag{17}$$

The strain time-derivative derivative can be directly calculated by the analytical differentiation of Eq. (16). After mathematical manipulations of each of these integrals (Eq. (16) and its time-derivative), for each Kelvin–Voigt element k, it yields the following numerical approximations (see Appendix):

$$\frac{\partial\varepsilon_{\mathrm{r}k}(x,t)}{\partial t} = \frac{J_k}{\tau_k}F(x,t) - \frac{\tilde{\varepsilon}_{\mathrm{r}k}(x,t)}{\tau_k} \tag{18}$$

$$\tilde{\varepsilon}_{\mathrm{r}k}(x,t) = J_k F(x,t) - J_k \mathrm{e}^{-\Delta t/\tau_k} F(x,t-\Delta t) - J_k\tau_k(1-\mathrm{e}^{-\Delta t/\tau_k})\frac{F(x,t)-F(x,t-\Delta t)}{\Delta t} + \mathrm{e}^{-\Delta t/\tau_k}\tilde{\varepsilon}_{\mathrm{r}k}(x,t-\Delta t) \tag{19}$$

Parameters J_k and τ_k are adjusted to the creep experimental data. The pipe diameter, wall-thickness and pipe-wall constraints coefficient are assumed constant and equal to initial values. Regarding the friction term h_{f} in Eq. (12), a second-order implicit scheme was used to calculate the steady-state component (Wylie and Streeter, 1993), and unsteady friction formulations were used to compute the unsteady component (Trikha's, Vardy's and Brunone's). Trikha's and Vardy's formulae are straightforwardly implemented by Eqs. (5a) and (5b). Brunone's formula requires the calculation of derivatives. A first-order explicit scheme was used to calculate the space derivative and a second-order implicit scheme for the time derivative, defined as follows, for the C^+ and C^- characteristic lines:

Local term

$$\left.\frac{\partial Q}{\partial t}\right|_{C\pm} = \theta\frac{Q(x,t)-Q(x,t-\Delta t)}{\Delta t} + (1-\theta)\frac{Q(x\mp\Delta x,t-\Delta t)-Q(x\mp\Delta x,t-2\Delta t)}{\Delta t} \tag{20}$$

Convective term

$$\left.\frac{\partial Q}{\partial x}\right|_{C\pm} = \frac{Q(x,t-\Delta t)-Q(x\mp\Delta x,t-\Delta t)}{\Delta x} \tag{21}$$

Sign term

$$SGN(Q)|_{C\pm} = SGN(Q(x\mp\Delta x,t-\Delta t)) \tag{22}$$

where θ is the relaxation coefficient. If $\theta = 0$, the flow time-derivative becomes explicit and, therefore, unstable for certain combinations of parameters; if $\theta > 0$, the numerical scheme is implicit and, thus, unconditionally stable. To minimize computer storage and increase computational speed, $\theta = 1$ was considered.

The flow parameters at section x and time t, Q and H, are calculated based on Eq. (12) for all interior sections of the pipes. At the ends of each pipe, additional equations (boundary conditions) have to be specified.

4 Model calibration and testing

4.1 Introduction

The developed mathematical model was calibrated and tested using with transient data collected from a PE pipe-rig at Imperial College (London, UK). The pipe has a length of 277 m and an inner diameter of 50.6 mm. There is a pressurized air vessel at the upstream end and a globe valve at the downstream. Transient events were generated by the fast closure of this valve. A complete description of the experimental facility and of the collected data can be found in the companion paper (Covas, 2004).

Four main approaches were followed to calibrate and test the developed transient solver. In the first two, the model was calibrated considering only one of the dynamic effects, either unsteady friction or pipe-wall viscoelasticity. In the third approach, the creep function was calibrated for laminar conditions using Trikha's formula and calibrated creep was used to calibrate and test the model for turbulent conditions. At last, the model was tested using the creep data experimentally determined in mechanical tests in the companion paper (Covas *et al.*, 2004).

With regard to steady state friction losses, the pipe-wall surface is smooth and the Darcy–Weisbach friction factor f_{s} is independent of pipe roughness. Friction is determined by the Hagen–Poiseuille formula for laminar flow, and by the Blasius formula for smooth-wall turbulent flows. Local head losses at elbows were estimated in 5% of friction losses (based on steady-state conditions).

4.2 Unsteady friction calibration neglecting pipe-wall viscoelasticity

In the first attempt to calibrate the transient solver, it was assumed that the pressure damping was only due to steady and unsteady friction (i.e. pipe-wall viscoelasticity was neglected). This is the normal procedure when using linear-elastic models. The transient event was simulated for laminar conditions ($Q_0 = 0.056$ l/s; $Re = 1400$) using Trikha's formula and the results are presented in Fig. 4. The classic waterhammer solution is presented in the same figure (for a wave speed, $a_0 = 385$ m/s). A major disagreement is observed between collected data and numerical results in terms of shape and extreme values of transient pressures. Trikha's formulation, which was considered a reasonable approximation of frictional dynamic effects in laminar flow, was not capable of describing the observed transient damping of the pressure surge. This meant that another phenomenon (not described by this formula) was occurring during the transient event.

A second attempt was made to describe the transient events for turbulent flow, both using Vardy's and Trikha's formulae and calibrating Brunone's decay coefficient (Fig. 5). In the same figure, the classic waterhammer solution is represented (for a wave speed, $a_0 = 385$ m/s).

Neither Trikha's nor the Reynolds dependent Vardy's formula could describe the observed damping of transient pressures in smooth-wall turbulent flows. Comparing Trikha's with Vardy's numerical results, it can be seen that unsteady friction effects are less important for turbulent conditions (if not negligible) than for laminar flows. This is according to what is expected, as Trikha's (or Zielke's) weighting function is an upper bound of Vardy's functions (Fig. 1b).

With regard to Brunone's formulation, an extremely high decay coefficient was calibrated to fit the numerical results with the observed extreme pressures. However, the shape of the pressure wave was still significantly different and, in no way, it could be represented by Brunone's formulation.

The general conclusion is that unsteady friction cannot thoroughly describe the attenuation and dispersion of transient pressures in polyethylene pipes.

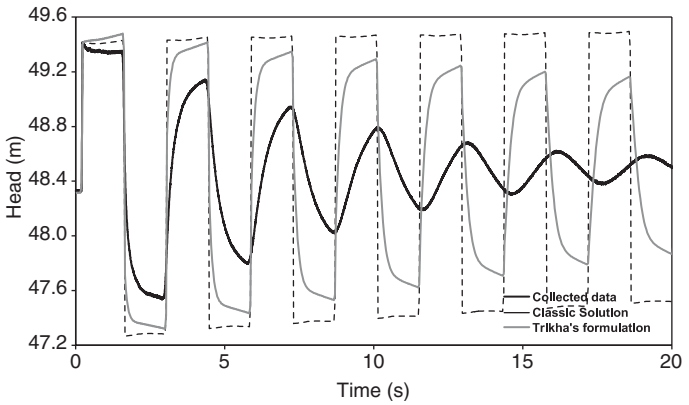

Figure 4 Piezometric head at Location 1. Experimental data versus numerical results considering only unsteady friction, for laminar conditions $Q_0 = 0.056$ l/s ($T = 20$°C).

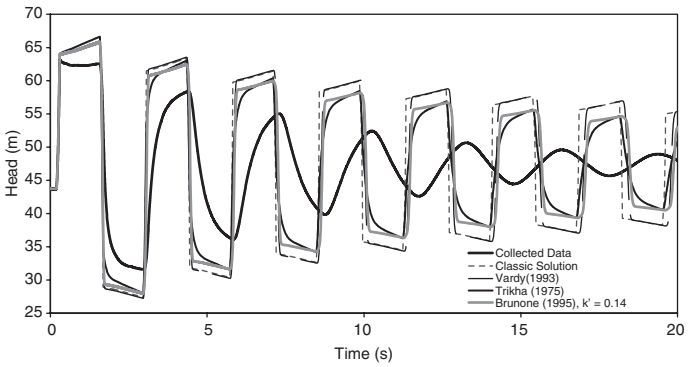

Figure 5 Piezometric head at Location 1. Experimental data versus numerical results considering only unsteady friction, for turbulent conditions $Q_0 = 1.0$ l/s ($T = 20$°C).

4.3 Creep calibration neglecting unsteady friction

The use of the viscoelastic transient solver requires as input data the description of the creep compliance function represented by the generalized Kelvin–Voigt model. This model is described by a set of parameters: the instantaneous elastic creep J_0 (i.e. a_0) and the retarded components, τ_k and J_k ($k = 1, \ldots, N_{KV}$ and N_{KV} = number of Kelvin–Voigt elements). If the creep $J(t)$ is unknown (the most probable case in engineering), this function has to be estimated (or calibrated) by adjusting the results of the numerical model to the transient data.

Unsteady-friction effects were neglected. Calibrations were carried out for several transient tests from laminar for smooth-wall turbulent flows ($Q_0 = 0.054$ l/s to $Q_0 = 1.98$ l/s). The creep function $J(t)$ was represented by several combinations of Kelvin–Voigt elements. The parameters τ_k and J_0 (i.e. a_0) were fixed before calibration. The parameters J_k were estimated by minimising the Least Square Error (LSE) between the calculated and measured piezometric head at transducer T1 located at the downstream end (Covas, 2003). Levenberg–Maquardt Algorithm was used to carry out the optimisation (Press *et al.*, 1988). A preliminary sensitivity analysis permitted to draw the following conclusions.

First, the wave speed a_0 was varied between 385 and 450 m/s according to the reference values presented in the companion paper. The higher the wave speed was, the smaller the lowest retardation time τ_k (i.e. τ_1) had to be to achieve the same accuracy (quantified by the LSE), and, consequently, the smaller the time-step Δt and the higher the computational time. Whilst, considering $a_0 < 400$ m/s, a good adjustment was obtained for $\tau_1 = 0.05$ s, when $a_0 = 425$ m/s was assumed, it would be necessary a $\tau_1 = 0.001$ s. The wave speed was fixed in 395 m/s as a compromise between accuracy and computational time.

For $a_0 = 395$ m/s (i.e. $J_0 = 0.70\text{E} - 9\,\text{Pa}^{-1}$ by Eq. (7) for $\alpha = 1.07$, $D = 50.6$ mm and $e = 6.3$ mm) and parameters τ_1 to τ_5 equal to 0.05, 0.5, 1.5, 5 and 10 s, respectively, a sensitivity analysis was carried out to obtain the optimal number of elements Kelvin–Voigt elements. Data corresponding to the initial flow $Q_0 = 1.0$ l/s were used. It was concluded that (see Table A-1), (i) the values of the calibrated J_k parameters varied with N_{KV} and the sample size ΔT, (ii) using $N_{KV} \geq 4$ did not

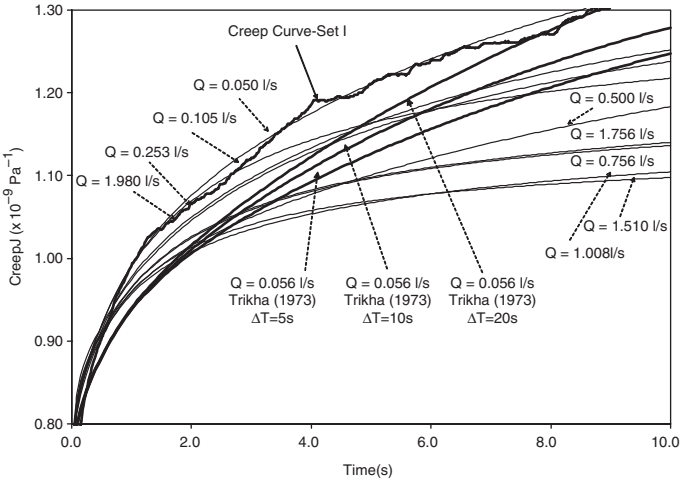

Figure 6 Calibrated creep functions for several flow rates neglecting unsteady friction.

improve the accuracy of the results (providing simply a different combination of J_k parameters), and (iii) the calibrated creep functions were significantly different from the experimental creep curve determined in the companion paper, but the higher N_{KV} the closer these were to the experimental creep function. $N_{\mathrm{KV}} = 5$ was used in order to better fit calibrated creep with measured creep function and not to improve the accuracy of the transient solver.

For the same set of parameters referred in the previous paragraph, calibration was carried out for different initial flows Q_0. Calibrated creep functions are presented in Fig. 6, as well the experimental creep function (*Set I*) determined in the companion paper. Each combination of parameters is one possible mechanical representation of the pipe creep. Different creep functions were obtained for each flow, though only one was supposed to exist. This is because unsteady friction (which is not accounted for in these simulations) has a similar dynamic effect on the pressure wave as pipe-wall viscoelasticity, as it attenuates the maximum pressure fluctuations and increases the dispersion of pressure wave. The only numerical way that the optimisation algorithm has to describe friction is by including it in the creep function (increasing the total creep). In fact, there is a resemblance between the frequency-dependent friction h_{fu} defined by Zielke (1968) and the frequency-dependent creep (Aklonis *et al.*, 1972), as both depend on the past-time histories of the fluid:

$$h_{\mathrm{fu}}(t) = \frac{16v'}{gD^2}\int_0^t \frac{\partial V(u)}{\partial t}\omega(t-u)\mathrm{d}u \quad \text{and}$$

$$\varepsilon_{\mathrm{r}}(t) = \frac{\alpha D}{2e}\int_0^t \frac{\partial p(u)}{\partial t}J(t-u)\mathrm{d}u$$

where $\omega(t)$ is the weighting function and $J(t)$ the creep function. The first term is incorporated in the momentum equation, whereas the second is in the continuity equation.

Numerical results obtained for $Q_0 = 1.0$ l/s are compared with the collected piezometric head and circumferential-strain time variation at Locations 1, 5 and 8 corresponding to distances from

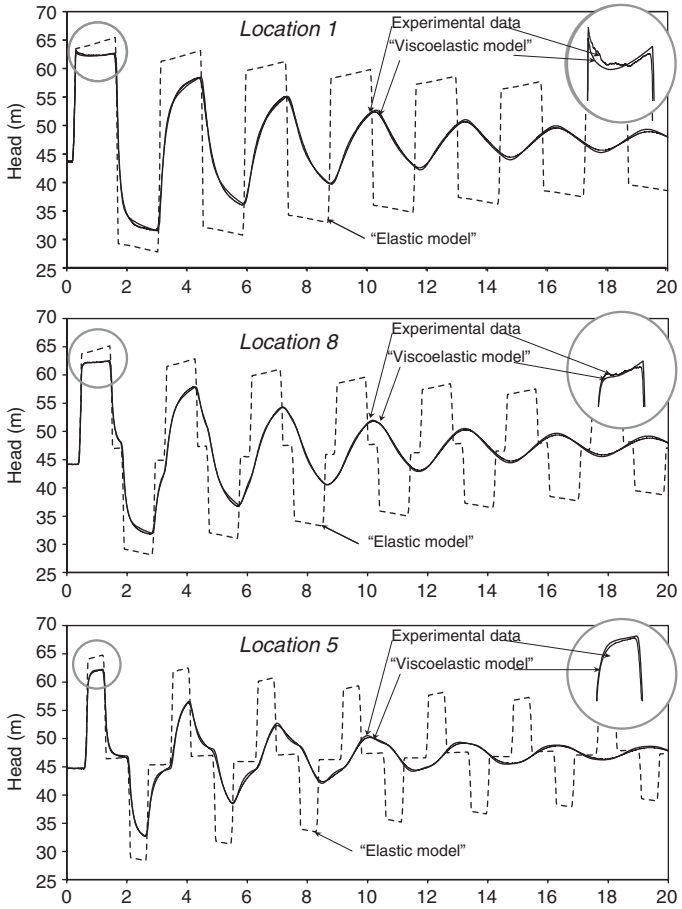

Figure 7 Piezometric head at Locations 1, 5 and 8 for $Q_0 = 1.0$ l/s ($T = 20$°C). Collected data versus numerical results for calibrated creep neglecting unsteady friction.

the upstream end of ∼271 m, ∼197 m and ∼116.5 m, respectively (Figs 7 and 8). Two numerical solutions for the piezometric head are presented. The first (dashed-line) was calculated using the 'elastic' waterhammer equations and the second (continuous-thin-line) the 'viscoelastic' equations. The classic waterhammer solution shows large discrepancies in both the pressure amplitude and phase with experimental data. These increase substantially with time and distance from the valve. The viscoelastic solution fits perfectly with the collected data. The retarded and the total strains are calculated as well by the numerical model considering the ratio inner/outer strain equal to 66% as determined in the companion paper. The retarded strain is one-fourth of the total strain. Calculated total strain agrees well with measured data (Fig. 8).

4.4 Calibration for laminar flow and verification/calibration for turbulent conditions

This approach can been classified as a two-step procedure: the first step consists of the creep function calibration for laminar conditions using Trikha's (1975) formula for unsteady friction effects, and the second step is the model verification for turbulent conditions by using Vardy's (1993) formulation or by calibrating Brunone's (1995) formula.

4.4.1 Calibration for laminar flow

The creep-function was calibrated for laminar conditions ($Q_0 = 0.056$ l/s; $Re = 1{,}400$) considering unsteady friction effects described by Trikha's formula (as this formula is considered to describe reasonably well the frictional dynamic effects). Though not accurate, Trikha's formula can be considered a good approximation of Zielke's exact formula for laminar conditions. The creep-function was calibrated for three sample sizes, $\Delta T = 5$, 10 and 20 s (see Table A-2 and Fig. 6). The larger the sample size, the higher calibrated creep is in time. This is possibly due to the increase in error of Trikha's formula with time, error that the calibrated creep function tends to compensate. Numerical results obtained for $\Delta T = 10$ s calibration are compared with collected data (Fig. 9).

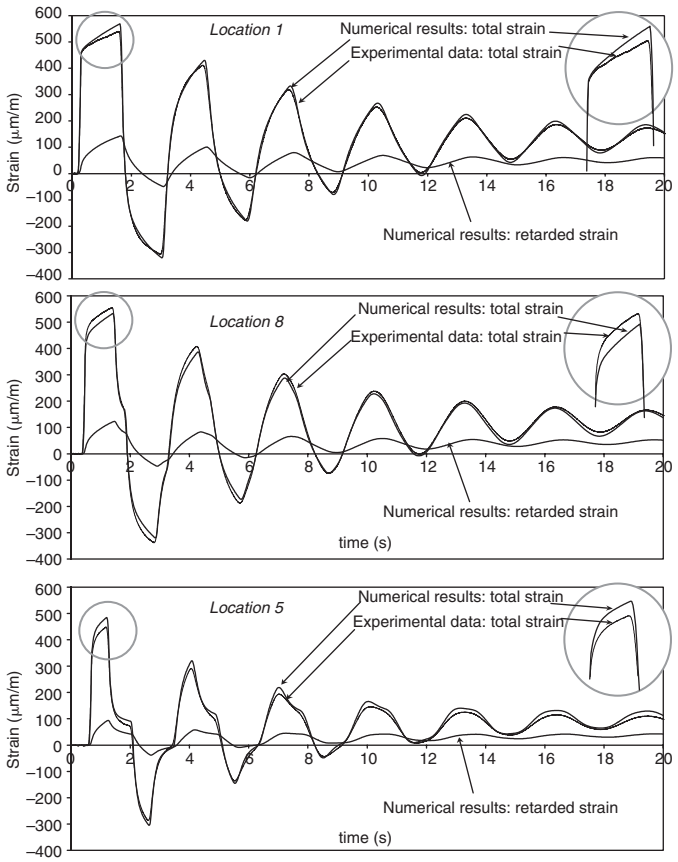

Figure 8 Circumferential strain at locations 1, 5 and 8 for $Q_0 = 1.0$ l/s ($T = 20$°C). Collected data versus numerical results for calibrated creep neglecting unsteady friction.

Three numerical solutions are presented: (i) classic waterhammer solution; (ii) results of the implementation of Trikha's formula only; and (iii) results of combination of pipe-viscoelasticity and unsteady friction. The latter results show good agreement with experimental data, which does not happen with the results of (i) and (ii).

4.4.2 Verification/calibration for smooth-wall turbulent conditions

Assuming a good approximation of the creep-function was achieved with the calibration for the laminar conditions for $\Delta T = 10$ s, this function was used for smooth-wall turbulent conditions ($Q_0 = 1.0$ l/s; $Re = 25{,}000$). Numerical results for six different cases are presented in Fig. 10: (i) the classic waterhammer solution; (ii) the implementation of Vardy's formula only; (iii) the implementation of Trikha's formula only; (iv) the implementation of Brunone's formula only with $k' = 0.03$; (v) Vardy's formula and viscoelasticity; and (vi) Brunone's formula and viscoelasticity. The following conclusions can be drawn:

- Unsteady friction cannot *per se* generate the total damping, phase-shift and curve-shape observed in transient pressures, as it can be seen in the solutions obtained without viscoelasticity using Trikha's, Vardy's and Brunone's formulations.
- Numerical results obtained combining unsteady friction models and viscoelasticity (calibrated for laminar conditions) fit very well with observed data. Brunone's formulation with $k' = 0.03$ combined with viscoelasticity lead to slightly higher damping than the observed data, whereas results obtained combining Vardy's with viscoelasticity fit very well with transient data.

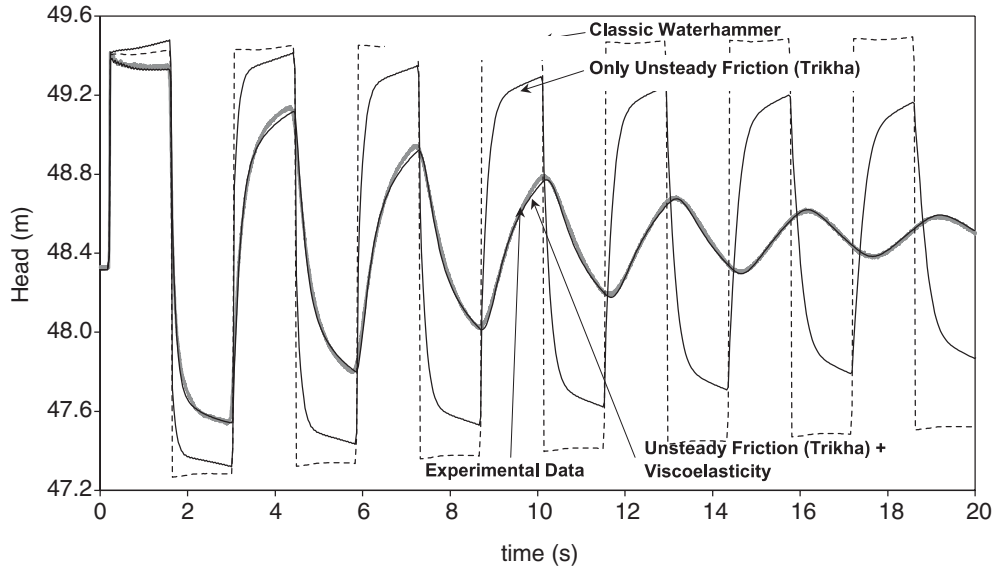

Figure 9 Piezometric head at Location 1 for laminar conditions, $Q_0 = 0.056$ l/s ($T = 20$°C). Collected data versus numerical results.

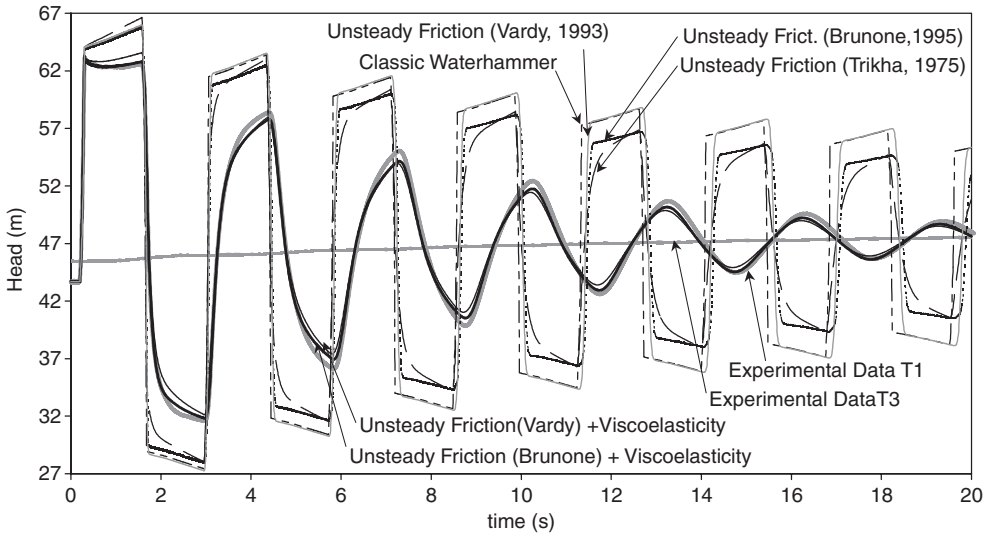

Figure 10 Piezometric head at Location 1 for smooth turbulent conditions, $Q_0 = 1.0$ l/s ($T = 20$°C). Collected data versus numerical results.

4.5 Model verification using creep data

Unsteady friction losses have a similar dynamic effect on pressure transients as the viscoelastic behaviour of the pipe-wall. The solution to distinguish these two overlapping phenomena is to isolate one of them and measure it in an independent test. With regard to unsteady friction, this phenomenon cannot be straightforwardly measured, particularly in PE pipes. Possible solutions could be the measurement of velocity profiles (Brunone *et al.*, 2000) or running the same transient tests in a metal or concrete pipe with linear-elastic walls. Concerning the viscoelastic behaviour of the PE, the creep function that characterizes this effect could be measured in mechanical tests with samples of pipe. This was the approach followed herein.

One of the creep functions, *Set I*, experimentally determined in Covas *et al.* (2004) has been used to test the model. Unsteady friction was neglected. The curve of the viscoelastic solid (Eq. 13) for the first 20 s was fitted to this creep function. A six-element Kelvin–Voigt model was considered with the following relaxation times τ_k: 0, 0.05, 0.50, 1.50, 5 and 10 s. The creep tests could not determine the elastic component J_0 of the creep function, nor precisely define the shape of the creep curve for ($t < 0.1$ s). Thus, several initial creep values J_0 were considered with wave speeds a_0 between 375 and 410 m/s. Calibrated creep coefficients are presented in Table A-3 and corresponding creep curves in Fig. 11. The results of the numerical simulations of the transient solver as well as collected data at transducer T1, for the steady-state flow $Q_0 = 1.0$ l/s, are presented in Fig. 12. Unsteady friction losses were neglected. Four main conclusions can be drawn from the analysis of these results.

First, the use of any of the experimentally determined creep curves improves the accuracy of the transient solver in comparison with the classic waterhammer solution for the linear elastic pipe. Second, the lower the initial J_0 is (the higher a_0), the higher is the viscoelastic component of creep, and, consequently, the more dissipation the pressure wave has and the more scatter of the numerical and measured results. Third, the best results are obtained for $a_0 = 395$ m/s ($J_0 = 0.7\,\text{GPa}^{-1}$), which means that this initial value is very close to the elastic component of creep. This value is consistent with the results of instantaneous wave

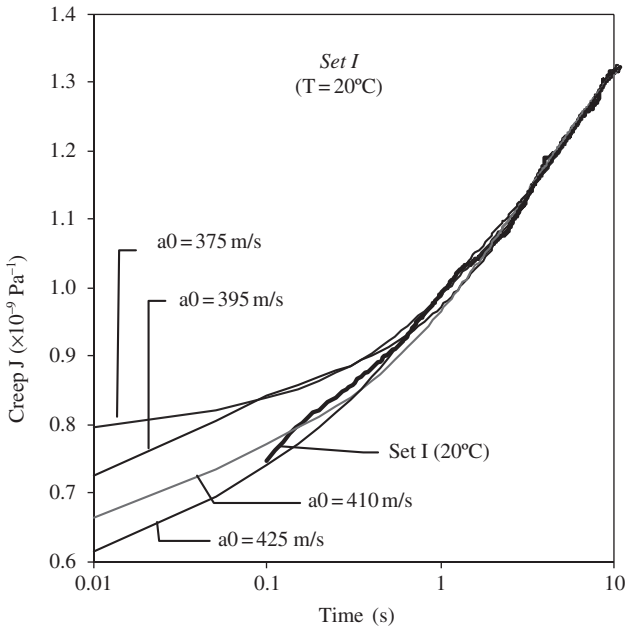

Figure 11 Representation of creep functions for several initial J_0 for data *Set I* ($T = 20$°C).

speed obtained in the companion paper (Covas *et al.*, 2004). Finally, none of the curves accurately represents the observed transient pressures, tending to generate lower pressure fluctuations. The PE in the pipe samples seems to be more flexible than the PE in the pipe-rig. The fact is that the pipe samples cannot accurately describe the overall constraints and stress-time history of the PE pipe-rig. These functions are good reference values of the real creep of the pipe, though they should be used with parsimony, as, in the current case, the generated overpressures are less severe than the observed values.

5 Summary and conclusions

The current paper presented a mathematical model for the calculation of waterhammer in PE pipes taking into account unsteady friction effects and the viscoelastic behaviour of pipe walls. The model was tested with experimental data. The strain-stress

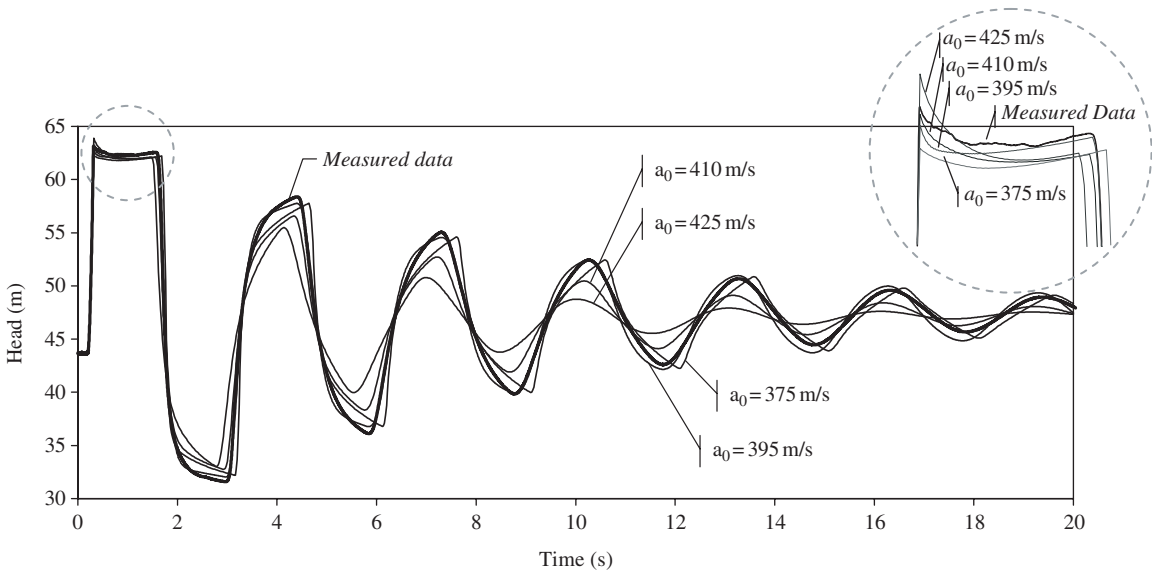

Figure 12 Piezometric head at Location 1 ($Q_0 = 1$ l/s): collected data versus numerical results ($T = 20$°C) based on creep data *Set I*.

relationship was determined by a creep-function. The numerical results obtained by the linear elastic and the linear viscoelastic models were compared with experimental data, neglecting and taking into account unsteady friction effects. The pressure-fluctuation obtained with the linear viscoelastic model showed a good agreement with the experimental data. Conversely, the pressure obtained by the classic solution showed a large discrepancy with the observed data. The circumferential strain was monitored and the results of the viscoelastic model fitted well with the data.

The major challenge of the current and the future work is the distinction between frictional and mechanical dampening. The viscoelastic behaviour of pipe walls has a dissipative and dispersive effect on the pressure wave, similar to unsteady friction losses. First, the two phenomena were analysed independently. Whilst unsteady friction could not represent the observed transient pressure, the creep function when calibrated without considering unsteady friction varied with the flow-rate. It was necessary to account for these two phenomena simultaneously. The distinction between these two effects can be achieved by measuring or calculating as accurately as possible one of them by: (i) calibrating creep-function based on collected data for laminar conditions considering Trikha's formulation and, later, testing the model for turbulent flows, (ii) determining the creep-function in an independent creep or dynamic mechanical test, or (iii) using more accurate models to simulate unsteady friction. The first two were followed herein. The main conclusion is that the developed viscoelastic solver is capable of accurately predicting transient pressures in PE pipes as long as creep is reasonably well described by the calibration based on laminar flows, or by mechanical tests.

Acknowledgments

The results presented here were achieved through a joint research project between the University of Exeter and Imperial College London supported by the UK Engineering and Physical Sciences Research Council (Inverse Transient Analysis for Pipe Roughness Calibration and Leak Detection). Additionally, Dídia Covas gratefully acknowledges the financial support of Fundação da Ciência e Tecnologia (FCT, Portugal) and Instituto Superior Técnico (IST, Portugal).

Appendix

Time-derivative of the retarded strain for each Kelvin–Voigt element k

The time-derivative of the retarded strain (Eq. 18) can be directly calculated by the analytical differentiation of Eq. (16) for each Kelvin–Voigt element k, as follows:

$$\begin{aligned}
\frac{\partial \varepsilon_{rk}(x,t)}{\partial t} &= \frac{d}{dt}\int_0^t F(x,t-t')\frac{J_k}{\tau_k}e^{-t'/\tau_k}dt' \\
&= \frac{d}{dt}\left(-\frac{J_k}{\tau_k}\int_t^0 F(x,y)e^{\frac{y-t}{\tau_k}}dy\right) \\
&= \frac{d}{dt}\left(\frac{J_k}{\tau_k}e^{-t/\tau_k}\int_0^t F(x,y)e^{y/\tau_k}dy\right) \\
&= -\frac{J_k}{\tau_k^2}e^{-t/\tau_k}\int_0^t F(x,y)e^{y/\tau_k}dy \\
&\quad + \frac{J_k}{\tau_k}e^{-t/\tau_k}\frac{d}{dt}\int_0^t F(x,y)e^{y/\tau_k}dy \\
&= -\frac{J_k}{\tau_k^2}e^{-t/\tau_k}\int_0^t F(x,y)e^{y/\tau_k}dy \\
&\quad + \frac{J_k}{\tau_k}e^{-t/\tau_k}F(x,y)e^{y/\tau_k} \\
&= -\frac{J_k}{\tau_k}\int_0^t F(x,y)\frac{e^{(y-t)/\tau_k}}{\tau_k}dy + \frac{J_k}{\tau_k}F(x,t) \\
&= -\frac{J_k}{\tau_k}\int_t^0 F(x,t-t')\frac{e^{-t'/\tau_k}}{\tau_k}(-1)dt' + \frac{J_k}{\tau_k}F(x,t) \\
&= -\frac{1}{\tau_k}\int_0^t F(x,t-t')\frac{J_k}{\tau_k}e^{\frac{-t'}{\tau_k}}dt' + \frac{J_k}{\tau_k}F(x,t) \\
\frac{\partial \varepsilon_{rk}(x,t)}{\partial t} &= -\frac{\varepsilon_{rk}(x,t)}{\tau_k} + \frac{J_k}{\tau_k}F(x,t) \qquad \text{(A1)}
\end{aligned}$$

Finite-difference scheme of the retarded strain for each Kelvin–Voigt element k

The numerical approximation of the retarded strain in Eq. (A1) can be defined by dividing the integral in Eq. (16) into two components and calculating these separately, as follows:

$$\varepsilon_{rk}(x,t) = \underbrace{\int_0^{\Delta t} F(x,t-t')\frac{J_k}{\tau_k}e^{-t'/\tau_k}dt'}_{\mathbf{A}} + \underbrace{\int_{\Delta t}^{t} F(x,t-t')\frac{J_k}{\tau_k}e^{-t'/\tau_k}dt'}_{\mathbf{B}} \tag{A2}$$

Term A

$$\mathbf{A} = \int_0^{\Delta t} F(x,t-t')\frac{J_k}{\tau_k}e^{-t'/\tau_k}dt'$$

$$\mathbf{A} = -\int_t^{t-\Delta t} F(x,t'')\frac{J_k}{\tau_k}e^{(t''-t)/\tau_k}dt''$$

$$\mathbf{A} = -F(x,t'')J_k e^{(t''-t)/\tau_k}\Big|_t^{t-\Delta t} + \int_t^{t-\Delta t}\frac{\partial F(x,t'')}{\partial t''}J_k e^{(t''-t)/\tau_k}dt''$$

$$\mathbf{A} = +J_k\left(F(x,t)-F(x,t-\Delta t)e^{-(\Delta t)/\tau_k}\right) + J_k\tau_k\frac{\partial F(x,t'')}{\partial t''}e^{(t''-t)/\tau_k}\Big|_t^{t-\Delta t} - \underbrace{\int_t^{t-\Delta t}\frac{\partial^2 F(x,t'')}{\partial t''^2}\tau_k e^{(t''-t)/\tau_k}dt''}_{\text{second order}\approx 0}$$

$$\tilde{\mathbf{A}} = +J_k\left(F(x,t)-F(x,t-\Delta t)e^{(-\Delta t)/\tau_k}\right) - J_k\tau_k\frac{F(x,t)-F(x,t-\Delta t)}{\Delta t}\left(1-e^{-(\Delta t)/\tau_k}\right) \tag{A3}$$

Term B

$$\mathbf{B} = \int_{\Delta t}^{t} F(x,t-t')\frac{J_k}{\tau_k}e^{-t'/\tau_k}dt'$$

$$\mathbf{B} = \int_0^{t-\Delta t} F(x,t-\Delta t-u)\frac{J_k}{\tau_k}e^{(-u-\Delta t)/\tau_k}du$$

$$\mathbf{B} = \varepsilon_{rk}(x,t-\Delta t)e^{(-\Delta t)/\tau_k} \tag{A4}$$

Introducing Eqs (A3) and (A4) into Eq. (A2), it yields Eq. (19).

In summary, the time-derivative of the retarded strain, $\partial\varepsilon_r/\partial t$, in characteristic equations (Eqs 12) is calculated by the sum of the time-derivative of the strain for each Kelvin–Voigt element $k\partial\varepsilon_{rk}/\partial t$ by Eq. (15). Each term $\partial\varepsilon_{rk}/\partial t$ is calculated by Eq. (18) as a function of the retarded strain ε_{rk}. The numerical approximation of the retarded strain ε_{rk} for each element k is given by Eq. (19).

Table A-1 Best fitted creep coefficients J_k for several K–V elements and sample sizes. Calibration for $Q_0 = 1.0081$/s neglecting unsteady friction ($a_0 = 395$ m/s)

Sample Size ΔT (s)	Number of K–V elements (−)	Creep coefficients J_k (Pa^{-1}) for the retardation times indicated below					Least Square Error (m^2)
		$\tau = 0.05$ s	$\tau = 0.5$ s	$\tau = 1.5$ s	$\tau = 5$ s	$\tau = 10$ s	
5	3	1.060E−10	9.330E−11	1.120E−10	—	—	0.0618
	3	1.060E−10	1.110E−10	—	2.390E−10	—	0.0591
	3	1.060E−10	1.140E−10	—	—	4.430E−10	0.0586
10	3	1.050E−10	1.040E−10	1.002E−10	—	—	0.0482
	3	1.043E−10	1.210E−10	—	2.196E−10	—	0.0474
	3	1.040E−10	1.240E−10	—	—	4.100E−10	0.0472
20	1	1.803E−10	—	—	—	—	17.2006
	2	8.494E−11	1.709E−10	—	—	—	0.1170
	3	1.044E−10	1.037E−10	1.145E−10	—	—	0.0611
	4	1.048E−10	1.029E−10	1.134E−10	8.083E−12	—	0.0610
	5	1.057E−10	1.054E−10	9.051E−11	2.617E−11	7.456E−11	0.0610
	3	1.355E−10	—	2.859E−10	1.555E−10	—	0.1991
	3	1.036E−10	1.230E−10	—	2.493E−10	—	0.0623
	3	1.035E−10	1.259E−10	—	—	4.655E−10	0.0626

Table A-2 Best fitted creep coefficients J_k for a four-element K–V model ($a_0 = 395\,\text{m/s}$). Calibration for laminar flow $Q_0 = 0.056\,\text{l/s}$ considering unsteady friction Trikha's formula

ΔT (s)	J_0 (10^{-9} Pa^{-1})	a_0 (m/s)	Creep coefficients J_k (10^{-9}Pa^{-1}) for the retardation times indicated below			Least Square Error (m^2)
			$\tau_1 = 0.05\,\text{s}$	$\tau_2 = 0.5\,\text{s}$	$\tau_3 = 10\,\text{s}$	
5	0.70	395	0.0804	0.1113	0.5456	0.00055
10	0.70	395	0.0805	0.1083	0.5763	0.00038
20	0.70	395	0.0801	0.1101	0.5906	0.00024

Table A-3 Best fitted creep coefficients J_k to represent experimental creep curve Set I (six-element K–V model)

J_0 (10^{-9} Pa^{-1})	a_0 (m/s)	Creep coefficients J_k (10^{-9} Pa^{-1}) for the retardation times indicated below					Least Square Error (10^{-9} Pa^{-2})
		$\tau_1 = 0.05\,\text{s}$	$\tau_2 = 0.5\,\text{s}$	$\tau_3 = 1.5\,\text{s}$	$\tau_4 = 5\,\text{s}$	$\tau_5 = 10\,\text{s}$	
0.79	372	0.0259	0.0712	0.1361	0.0122	0.4526	0.101
0.75	381	0.0333	0.1621	0.0214	0.1972	0.2925	0.092
0.70	394	0.1394	0.0062	0.1148	0.3425	0.0928	0.110
0.64	410	0.1092	0.0912	0.1554	0.2695	0.1339	0.091
0.59	426	0.1010	0.2632	0.0101	0.2639	0.1935	0.066

Notation

a_0 = elastic wave speed (m/s)
D = pipe inner diameter (m)
D_0 = initial pipe inner diameter (m)
e = pipe-wall thickness (m)
e_0 = initial pipe-wall thickness (m)
E_0 = Young's modulus of elasticity of the pipe (Pa)
E_k = Young's modulus of elasticity of the springs (Pa)
f_s = Darcy–Weisbach steady-state friction factor (–)
g = gravity due to acceleration (m/s^2)
h_f = head loss per unit length (–)
h_{fs} = steady-state component of the head loss per unit length (–)
h_{fu} = unsteady-state component of the head loss per unit length (–)
H = piezometric-head, $H = p/\gamma + z$ (m)
H_0 = steady-state piezometric head (m)
J = creep-compliance (Pa^{-1})
J_0 = instantaneous or elastic creep-compliance (Pa^{-1})
J_k = creep of the springs of the Kelvin–Voigt elements, $J_k = 1/E_k$ (Pa^{-1})
K = bulk modulus of elasticity of the fluid (Pa)
L = length of the pipeline (m)
n = exponent of flow in the friction loss equation (–)
N_{KV} = number of Kelvin–Voigt elements (–)
p = pressure of the fluid (Pa)
p_0 = initial steady-state pressure (Pa)
Q = flow-rate (m^3/s)
Q_0 = initial steady-state flow-rate (m^3/s)
Re = Reynolds number, $Re = VD/\nu'$ (–)
S = pipe cross-section (m^2)
T = temperature of the fluid; period of pressure wave, $T = 4L/a$ (s)
t, t', t'' = time (s)
V = average velocity of the fluid (m/s)
x = coordinate along the pipe axis (m)
ρ = fluid density (kg/m^3)
α = dimensionless parameter (function of pipe cross-section dimensions and constraints) (–)
θ = weighting coefficient for the flow-time derivative calculation (–)
ν = Poisson's ratio (ratio between axial and circumferential strain) (–)
ν' = kinematic fluid viscosity (m^2/s)
ε = strain; circumferential total strain (m/m)
ε_0 = initial strain (m/m)
ε_i = strain (m/m)
ε_e = instantaneous-elastic strain (m/m)
ε_r = retarded strain (m/m)
σ = stress; circumferential-stress (Pa)
σ_0 = initial stress (Pa)
τ_k = retardation time of the dashpots, $\tau_k = \eta_k/E_k$ (s)
η_k = the viscosity of the dashpots (kg/sm)
Δt = time-step increment (s)
ΔT = sample length used for calibration (s)
Δx = space-step increment (m)

References

1. AKLONIS, J.J., MACKNIGHT, W.J. and SHEN, M. (1972). *Introduction to Polymer Viscoelasticity.* John Wiley & Sons, Inc., New York.

2. ALMEIDA, A.B. and KOELLE, E. (1992). *Fluid Transients in Pipe Networks.* Computational Mechanics Publications. Elsevier Applied Science, Amsterdam.
3. BERGANT, A., SIMPSON, A. R. and VITKOVSKY, J.P. (2001). "Developments in Unsteady Pipe Flow Friction Modelling". *J. Hydraul. Res., IAHR* 39(3), 249–257.
4. BRATLAND, O. (1986). "Frequency-Dependent Friction and Radial Kinetic Energy Variation in Transient Pipe Flows". *Proceedings of 5th International Conference on Pressure Surges.* BHR Group Ltd., Hanover, Germany, pp. 95–101.
5. BRUNONE, B., GOLIA, U.M. and GRECO, M. (1991). "Some Remarks on the Momentum Equation for Fast Transients". *Proceedings of the International Conference on Hydraulic Transients with Water Column Separation (9th and Last Round Table of IAHR Group)*, Valencia, Spain, pp. 201–209.
6. BRUNONE, B., GOLIA, U.M. and GRECO, M. (1995). "Effects of Two-Dimensionality on Pipe Transients Modelling". *J. Hydraul. Engng., ASCE* 121(12), 906–912.
7. BRUNONE, B., KARNEY, B. and FERRANTE, M. (1999). "Velocity Profiles, Unsteady Friction Losses and Transient Modelling". *26th Water Resources Planning and Management Conference.* ASCE, Tempe, Arizona.
8. BRUNONE, B., KARNEY, B., MERCARELLI, M. and FERRANTE, M. (2000). "Velocity Profiles and Unsteady Pipe Friction in Transient Flow". *J. Water Resour. Planning Mgmt*., ASCE 126(4), 236–244.
9. CARSTENS, M.R. and ROLLER, J.E. (1959). "Boundary-Shear Stress in Unsteady Turbulent Pipe Flow". *J. Hydraul. Div., ASCE* 85(HY2), 67–81.
10. CHAUDHRY, M.H. (1987). *Applied Hydraulic Transients*, 2nd ed. Litton Educational Publishing Inc., Van Nostrand Reinhold Co., New York.
11. COVAS, D. (2003). "Inverse Transient Analysis for Leak Detection and Calibration of Water Pipe Systems—Modelling Special Dynamic Effects". PhD Thesis, Imperial College of Science, Technology and Medicine, University of London, London, UK.
12. COVAS, D., STOIANOV, I., MANO, J., RAMOS, H., GRAHAM, N. and MAKSIMOVIC, C. (2004). "The Dynamic Effect of Pipe-Wall Viscoelasticity in Hydraulic Transients. Part I—Experimental Analysis and Creep Characterization". *J. Hydraul. Res., IAHR* 42(5), 516–530.
13. DAILY, J.W., HANKEY, Jr. W.L., OLIVE, R.W. and JORDAN, Jr. J.M. (1956). "Resistance Coefficients for Accelerated and Decelerated Flows Through Smooth Tubes and Orifices". *J. Basic Engng. Trans. ASME, Ser. D* 78(7), 1071–1077.
14. EICHINGER, P. and LEIN, G. (1992). "The Influence of Friction on Unsteady Pipe Flow". *Proceedings of the International Conference on Unsteady Flow and Fluid Transients.* Bettess & Watts, Balkema, Rotterdam, pp. 41–50.
15. FERRY, J.D. (1970). *Viscoelastic Properties of Polymers*, 2nd edn. John Wiley & Sons, New York.
16. FRANKE, G. and SEYLER, F. (1983). "Computation of Unsteady Pipe Flow with Respect to Viscoelastic Material Properties". *J. Hydraul. Res., IAHR* 21(5), 345–353.
17. GALLY, M., GUNEY, M. and RIEUTFORD, E. (1979). "An Investigation of Pressure Transients in Viscoelastic Pipes". *J. Fluid Engng., Trans. ASME* 101, 495–499.
18. GHILARDI, P. and PAOLETTI, A. (1986). "Additional Viscoelastic Pipes as Pressure Surge Suppressors". *Proceedings of 5th International Conference on Pressure Surges.* BHR Group Ltd., Hannover, Germany, pp. 113–121.
19. HINO, M., SAWAMOTO, M. and TAKASU, S. (1976). "Experiments on Transition to Turbulence in an Oscillatory Pipe Flow". *J. Fluid Mech.* 75(2), 193–207.
20. HINO, M., SAWAMOTO, M. and TAKASU, S. (1977). "Study on the Transition to Turbulence and Frictional Coefficient in an Oscillatory Pipe Flow". *Trans. JSCE* 9, 282–285.
21. HOLMBOE, E.L. and ROULEAU, W.T. (1967). "The Effects of Viscous Shear on Transients in Liquid Lines". *J. Basic Engng., Trans. ASME, Ser. D* 89(1), 174–180.
22. MEIßNER, E. and FRANKE, G. (1977). "Influence of Pipe Material on the Dampening of Waterhammer". *Proceedings of the 17th Congress of the International Association for Hydraulic Research.* IAHR, Baden-Baden, Germany.
23. PEZZINGA, G. (1999). "Quasi-2D Model for Unsteady Flow in Pipe Networks". *J. Hydraul. Engng., ASCE* 125(7), 676–685.
24. PEZZINGA, G. (2000). "Evaluation of Unsteady Flow Resistances by Quasi-2D and 1D Models". *J. Hydraul. Engng., ASCE* 126(10), 778–785.
25. PEZZINGA, G. (2002). "Unsteady Flow in Hydraulic Networks with Polymeric Additional Pipe". *J. Hydraul. Engng., ASCE* 128(2), 238–244.
26. PRESS, W.H., FLANNERY, B.P., TEUKOLSKY, S.A. and VETTERLING, W.T. (1988). *Numerical Recipes in C.* Cambridge University Press, Cambridge.
27. RACHID, F.B.F., MATTOS, H.C. and STUCKENBRUCK, S. (1992). "Waterhammer in Inelastic Pipes: an approach via Internal Variable Constitutive Theory". In: BETTESS and WATTS (eds), *Proceedings of the International Conference on Unsteady Flow and Fluid Transients.* Balkema, Rotterdam, pp. 63–70.
28. RACHID, F.B.F. and STUCKENBRUCK, S. (1990). "Transients in Liquid and Structure in Viscoelastic Pipes". *Proceedings of the 6th International Conference on Pressure Surges.* BHR Group Ltd, Cranfield, UK, pp. 69–84.
29. RIANDE, E., DÍAZ-CALLEJA, R., PROLONGO, M.G., MASEGOSA, R.M. and SALOM, C. (2000). *Polymer Viscoelasticity: Stress and Strain in Practice.* Marcel Dekker, Inc., New York.
30. RIEUTFORD, E. (1982). "Transients Response of Fluid Viscoelastic Lines". *J. Fluid Engng., ASME* 104, 335–341.
31. RIEUTFORD, E. and BLANCHARD, A. (1979). "Ecoulement Non-permanent en Conduite Viscoelastique—Coup de Bélier". *J. Hydraul. Res., IAHR* 17(1), 217–229.

32. SAFWAT, H. and POLDER, J. (1973). "Friction-Frequency Dependence for Oscillatory Flows in Circular Pipes". *J. Hydraul. Div., ASCE* HY11, November 1933–1945.
33. SHUY, E.B. (1996). "Wall Shear Stress in Accelerating and Desacelerating Turbulent Pipe Flows". *J. Hydraul. Res., IAHR* 34(2).
34. SILVA-ARAYA, W.F. and CHAUDHRY, M.H. (1997). "Computation of Energy Dissipation in Transient Flow". *J. Hydraul. Engng., ASCE* 123(2), 108–115.
35. SUO, L. and WYLIE, E.B. (1990a). "Complex Wave Speed and Hydraulic Transients in Viscoelastic Pipes". *J. Fluid Engng., Trans. ASME* 112, 496–500.
36. SUO, L. and WYLIE, E.B. (1990b). "Hydraulic Transients in Rock-Bored Tunnels". *J. Hydraul. Engng., ASCE* 116(2), 196–210.
37. SUZUKI, K., TAKETOMI, T. and SATO, S. (1991). "Improving Zielke's Method of Simulating Frequency-Dependent Friction in Laminar Liquid Pipe Flow". *J. Fluids Engng., Trans. ASME* 113(4), 569–573.
38. TRIKHA, A.K. (1975). "An Efficient Method for Simulating Frequency-Dependent Friction in Transient Liquid Flow". *J. Fluids Engng., Trans. ASME* 97(1), 97–105.
39. VARDY, A.E. (1992). "Approximating Unsteady Friction at High Reynolds Numbers". In: BETTESS and WATTS (eds), *Proceedings of the International Conference on Unsteady Flow and Fluid Transients*. Balkema, Rotterdam, pp. 21–29.
40. VARDY, A.E. and BROWN, J. (1995). "Transient, Turbulent, Smooth Pipe Friction". *J. Hydraul. Res., IAHR* 33(4), 435–456.
41. VARDY, A.E. and BROWN, J. (1996). "On Turbulent, Unsteady, Smooth-Pipe Friction". *Proceedings of the 7th International Conference on Pressure Surges and Fluid Transients in Pipelines and Open Channels.* BHR Group Ltd., Harrogate, UK, pp. 289–311.
42. VARDY, A.E. and HWANG, K.L. (1991). "A Characteristic Model of Transient Friction in Pipes". *J. Hydraul. Res., IAHR* 29(5), 669–684.
43. VARDY, A.E., HWANG, K.L. and BROWN, J. (1993). "A Weighting Function Model of Transient Turbulent Pipe Friction". *J. Hydraul. Res., IAHR* 31(4), 533–548.
44. VITKOVSKY, J.P., LAMBERT, M.F. and SIMPSON, A.R. (2000). "Advances in Unsteady Friction Modelling in Transient Pipe Flow". *Proceedings of the 8th International Conference on Pressure Surges.* BHR Group Ltd., The Hague, The Netherlands, pp. 471–498.
45. WYLIE, E.B. and STREETER, V.L. (1993). *Fluid Transients in Systems.* Prentice Hall, Englewood Cliffs, NI.
46. ZIELKE, W. (1968). "Frequency-Dependent Friction in Transient Pipe Flow". *J. Basic Engng., Trans. ASME, Ser. D* 90(1), 109–115.